Comput Visual Sci (2009) 12:329–336
DOI 10.1007/s00791-008-0111-3

REGULAR ARTICLE

Modelling and simulation of moving contact line problems with wetting effects

Sashikumaar Ganesan · Lutz Tobiska

Received: 31 January 2007 / Accepted: 14 August 2007 / Published online: 12 April 2008
© Springer-Verlag 2008

Abstract This paper presents a numerical scheme for computing moving contact line flows with wetting effects. The numerical scheme is based on Arbitrary Lagrangian Eulerian (ALE) finite elements on moving meshes. In the computations, the wetting effects are taken into account through a weak enforcement of the prescribed equilibrium contact angle into the model equations. The equilibrium contact angle is included in the variational form of the model by replacing the curvature with Laplace Beltrami operator and integration by parts. This weak implementation allows that the contact angle determined by the numerical scheme differs from the equilibrium value and develops a certain dynamics. The Laplace Beltrami operator technique with an interface/boundary resolved mesh is well-suited for describing the dynamic contact angle observed in experiments. We consider the spreading and the pendant liquid droplets to investigate this implementation of the contact angle. It is shown that the dynamic contact angle tends to the prescribed equilibrium contact angle when time goes to infinity. However, the dynamics of the contact angle is influenced by the slip at the moving contact line.

Communicated by P. Frolkovic.

This work has been partially supported by the German Research Foundation (DFG) through the grant To143/9.

S. Ganesan (✉) · L. Tobiska
Institut für Analysis und Numerik,
Otto-von-Guericke-Universität Magdeburg,
Postfach 4120, 39016 Magdeburg, Germany
e-mail: ga.sashikumaar@mathematik.uni-magdeburg.de

L. Tobiska
e-mail: lutz.tobiska@mathematik.uni-magdeburg.de

1 Introduction

In free surface and interface flows, the contact points (in 2D) or contact line (in 3D) emerges when the interface between a liquid–gas or a liquid–liquid intersects a solid surface. The contact line is said to be a moving contact line if the relative velocity between the interface and the solid surface is non-zero, i.e., the interface and solid surface move (either one of these two can be also fixed) in different velocities. In computations of these type of flows, the description of an appropriate boundary condition at the moving contact line and the inclusion of the wetting effect, i.e., inclusion of the contact angle, are the two main difficulties.

Using the no-slip condition at the moving contact line leads to an non-integrable force singularity in the model. Several boundary conditions have been proposed in the literature to relieve this singularity, see for an overview [4,7]. Among them, the so-called Navier-slip boundary condition has been more often used and is widely accepted. It reads:

$$\mathbf{u}\cdot\boldsymbol{\nu}_S = 0, \quad \mathbf{u}\cdot\boldsymbol{\tau}_{i,S} = -\epsilon_\mu(\boldsymbol{\tau}_{i,S}\cdot\mathbb{T}(\mathbf{u},p)\cdot\boldsymbol{\nu}_S) \tag{1}$$

for $i = 1,\ldots,d-1$, on the liquid–solid interface. Here, d is the dimension of the considered problem, $\boldsymbol{\nu}_S$ and $\boldsymbol{\tau}_{i,S}$ are the unit normal and tangential vectors on the liquid–solid interface. Further, ϵ_μ is the slip coefficient. The unit of the stress tensor $\mathbb{T}(\mathbf{u},p)$ is kg/(m s^2) and the velocity is m/s. Thus, from the dimensional analysis, the unit of the slip coefficient ϵ_μ should be of $\epsilon\mu_0^{-1}$, where ϵ and μ_0 have the unit of a length and a dynamic viscosity, respectively. The first condition in (1) is the no penetration boundary condition, that is, the fluid cannot penetrate into an impermeable solid and thus the normal component of the velocity is zero. The second condition is the slip with friction boundary condition, that is, on the liquid–solid interface, the tangential velocities of the fluid are proportional to their corresponding tangential

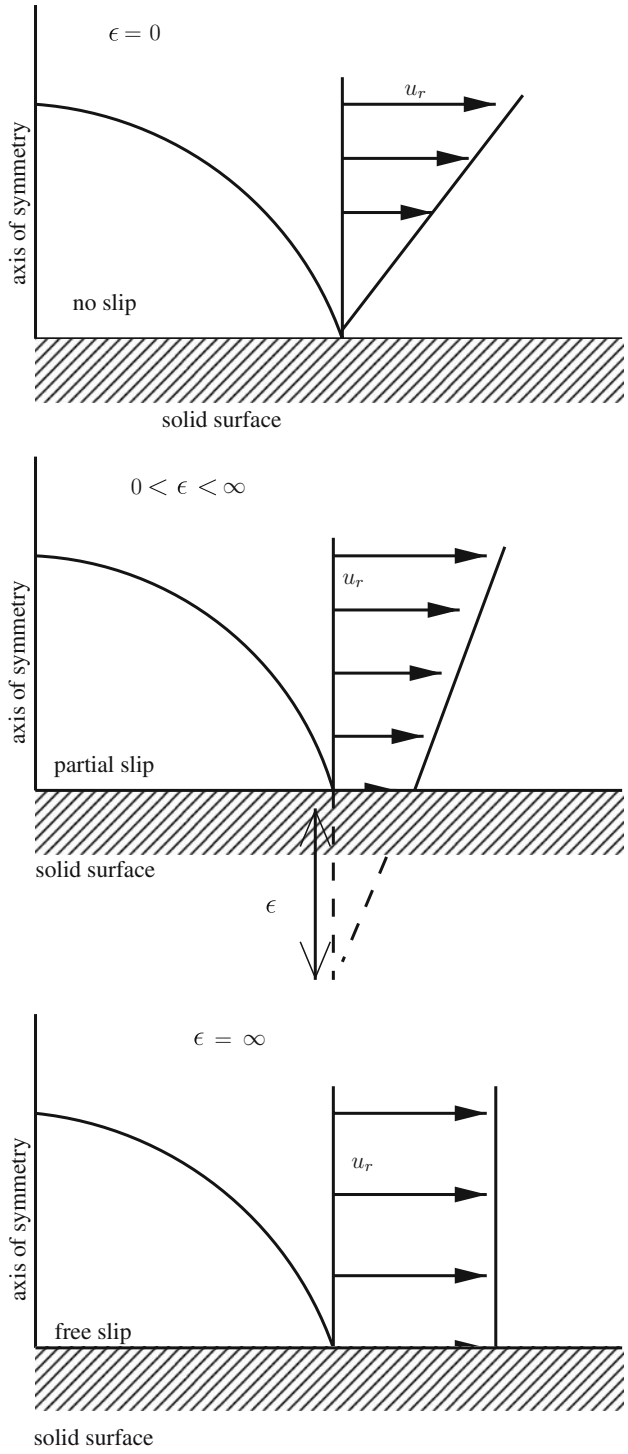

Fig. 1 Interpretation of the slip-length ϵ. *Arrows* indicate the magnitude of the velocity component in X direction

stress. Depending on the choice of ϵ, we get different types of boundary conditions as:

1. no-slip if $\epsilon = 0$,
2. slip with friction if $0 < \epsilon < \infty$,
3. free slip if $\epsilon = \infty$.

For an interpretation of the slip-length, see Fig. 1. For example, in case of shear flow, i.e., partial slip, ϵ can be interpreted [7] as the fictitious distance to the solid surface as shown in Fig. 1 (middle). In our model, we use the second type, i.e., the slip with friction type condition.

Next, to include the wetting effects, a description of the contact angle (the angle formed between the liquid–gas interface and the liquid–solid interface) has to be included to the flow equations. Earlier, Fukai et al. [5] included the contact angle into the model through the curvature approximation at the contact line in their Lagrangian approach computations of a spreading droplet. In the volume-of-fluid approach, Renardy et al. [9] have preferred to incorporate the contact angle while determining the normal to the interface at the solid surface. Alternatively, the contact angle has been included as local force into the model equations by Sikalo et al. [12] in their volume-of-fluid approach. Recently, in the level set approach Spelt [11] has imposed the contact angle condition in the redistance step of level set function after solving the flow equations. In this paper, we present a new finite element scheme for the moving contact line problem which includes the contact angle as an input parameter in the weak form of the model equations, which allows different choices, for example, the equilibrium, the advancing or the receding contact angle. In our numerical tests, we will always set this input parameter equal to the equilibrium contact angle.

2 Finite element model

In our study the considered test examples of moving contact line problems are the spreading and pendant axisymmetric liquid droplets. The finite element model for these moving contact line problems is presented in this section. We will only simulate the liquid phase where the influence of the gas phase is neglected.

2.1 Governing equations

The fluid flow in the liquid droplet is governed by the time dependent Navier–Stokes equations in a time dependent domain $\Omega(t) \subset \mathbb{R}^3$. In the time interval (0, I] the dimensionless form of the model equations reads:

$$\begin{aligned} \frac{\partial \mathbf{u}}{\partial t} + (\mathbf{u} \cdot \nabla)\mathbf{u} - \nabla \cdot \mathbb{S}(\mathbf{u}, p) &= \frac{1}{Fr}\,\mathbf{e} \quad \text{in } \Omega(t), \\ \nabla \cdot \mathbf{u} &= 0 \qquad \text{in } \Omega(t), \end{aligned} \tag{2}$$

where the dimensionless stress tensor $\mathbb{S}(\mathbf{u}, p)$ and the velocity deformation tensor $\mathbb{D}(\mathbf{u})$ are given by

$$\mathbb{S}(\mathbf{u}, p) = \frac{2}{Re}\mathbb{D}(\mathbf{u}) - p\mathbb{I},$$
$$\mathbb{D}(\mathbf{u}) = \frac{1}{2}\left(\nabla \mathbf{u} + \nabla \mathbf{u}^T\right).$$

Here, $\mathbf{u}$ is the fluid velocity, p the pressure in the fluid, t the time, $\mathbf{e}$ an unit vector in the opposite direction of the gravitational force and $\mathbb{I}$ the identity tensor. Further, ∇ denotes the gradient operator, $\nabla\cdot$ denotes the divergence operator and the superscript T denotes the transpose. The Reynolds number and the Froude number are given by

$$Re = \frac{\rho U L}{\mu}, \quad Fr = \frac{U^2}{Lg},$$

where L is the characteristic length, U the characteristic velocity, ρ the density, μ the dynamic viscosity and g the gravitational constant.

2.2 Boundary conditions for flows with a moving contact line

The force balancing and kinematic conditions are used on the free surface $\Gamma_F(t)$. As discussed in the introduction the Navier-slip boundary condition is imposed on the liquid–solid interface $\Gamma_S(t)$. The dimensionless form of the boundary conditions in (0, I] reads:

$$\begin{aligned}
\boldsymbol{\nu}_F \cdot \mathbb{S}(\mathbf{u}, p) \cdot \boldsymbol{\nu}_F &= \frac{\mathcal{K}}{We} && \text{on } \Gamma_F(t),\\
\boldsymbol{\tau}_{i,F} \cdot \mathbb{S}(\mathbf{u}, p) \cdot \boldsymbol{\nu}_F &= 0 && \text{on } \Gamma_F(t),\\
\mathbf{u} \cdot \boldsymbol{\nu}_F &= \mathbf{w} \cdot \boldsymbol{\nu}_F && \text{on } \Gamma_F(t),\\
\mathbf{u} \cdot \boldsymbol{\nu}_S &= 0 && \text{on } \Gamma_S(t),\\
\beta_\epsilon(\boldsymbol{\tau}_{i,s} \cdot \mathbb{S}(\mathbf{u}, p) \cdot \boldsymbol{\nu}_s) &= -\mathbf{u} \cdot \boldsymbol{\tau}_{i,S} && \text{on } \Gamma_S(t),
\end{aligned} \tag{3}$$

for $i = 1, 2$. Here, $\boldsymbol{\nu}_F$ and $\boldsymbol{\tau}_{i,F}$ are the unit normal and tangential vectors, respectively on the free surface. Further, $\mathcal{K}$ is the sum of the principal curvatures and $\mathbf{w}$ is the free surface velocity. The dimensionless numbers (Weber and slip, respectively) in the above equations are defined by

$$We = \frac{\rho U^2 L}{\sigma}, \quad \beta_\epsilon = \epsilon_\mu \rho U,$$

where σ is the coefficient of surface tension.

In addition to these boundary conditions (3), the contact angle θ at the contact line has to be prescribed. A simple form is to prescribe the contact angle as the equilibrium contact angle θ_e, i.e., $\theta = \theta_e$. A more general form is to prescribe the contact angle with respect to the contact line velocity $\mathbf{u}^{cl}$ as

$$\begin{aligned}
\theta &= \theta_A && \text{if } \mathbf{u}^{\mathrm{cl}} > 0,\\
\theta &= \theta_R && \text{if } \mathbf{u}^{\mathrm{cl}} < 0,\\
\theta_R \le \theta &\le \theta_A && \text{if } \mathbf{u}^{\mathrm{cl}} = 0.
\end{aligned}$$

Here, θ_A and θ_R are the advancing and receding contact angles, respectively. One could also use any experimentally validated law depending on the contact line velocity.

2.3 Inclusion of the contact angle

To include the contact angle, we start with the weak form of the model (2). Let $V := (H^1(\Omega(t)))^3$ and $Q := L^2(\Omega(t))$ be the usual Sobolev spaces. We multiply (2) by test functions $\mathbf{v} \in V$ and $q \in Q$ and integrate over $\Omega(t)$. After integrating by parts and incorporating the boundary conditions, the weak form of (2) reads:

For given $\Omega(0)$ and $\mathbf{u}(0)$, find $(\mathbf{u}(t), p(t)) \in V \times Q$ such that

$$\left(\frac{\partial \mathbf{u}}{\partial t}, \mathbf{v}\right) + a(\mathbf{u}; \mathbf{u}, \mathbf{v}) - b(p, \mathbf{v}) + b(q, \mathbf{u}) = f(\mathcal{K}, \mathbf{v}), \tag{4}$$

for all $\mathbf{v} \in V$ and $q \in Q$. Here,

$$\begin{aligned}
a(\hat{\mathbf{u}}; \mathbf{u}, \mathbf{v}) &= \frac{2}{Re} \int_{\Omega(t)} \mathbb{D}(\mathbf{u}) : \mathbb{D}(\mathbf{v})\, dx \\
&\quad + \int_{\Omega(t)} (\hat{\mathbf{u}} \cdot \nabla)\mathbf{u} \cdot \mathbf{v}\, dx \\
&\quad + \frac{1}{\beta_\epsilon} \int_{\Gamma_S(t)} (\mathbf{u} \cdot \boldsymbol{\tau}_{i,S})(\mathbf{v} \cdot \boldsymbol{\tau}_{i,S})\, d\gamma_S,\\
b(q, \mathbf{v}) &= \int_{\Omega(t)} q\, \nabla \cdot \mathbf{v}\, dx,\\
f(\mathcal{K}, \mathbf{v}) &= \frac{1}{Fr} \int_{\Omega(t)} \mathbf{e} \cdot \mathbf{v}\, dx \\
&\quad + \frac{1}{We} \int_{\Gamma_F(t)} (\mathbf{v} \cdot \boldsymbol{\nu}_F)\, \mathcal{K}\, d\gamma_F.
\end{aligned}$$

Now, the contact angle is included by replacing the curvature $\mathcal{K}$ in the free surface integral with the Laplace Beltrami operator and then integration by parts. The Laplace Beltrami operator is defined as the tangential divergence of the tangential gradient $\underline{\nabla}$, i.e., for a scalar function h,

$$\underline{\Delta}(h) := \underline{\nabla} \cdot \underline{\nabla}(h),$$

where,

$$\underline{\nabla}(h) := \nabla(h) - (\boldsymbol{\nu}_F \cdot \nabla(h))\boldsymbol{\nu}_F.$$

This technique of reducing the order of differentiation associated with the curvature term has been already employed in [10]. The formulation by means of the Laplace Beltrami operator has been proposed in [3] and was also used in [1,8] for flows within a closed free surface, i.e., flows without moving contact lines. Here, we extend this technique for

flows with moving contact lines as

$$\begin{aligned}\frac{1}{We}\int_{\Gamma_F(t)} \mathbf{v}\cdot\boldsymbol{\nu}_F\mathcal{K}\,d\gamma_F &= \frac{1}{We}\int_{\Gamma_F(t)} \underline{\Delta} id_{\Gamma_F}\cdot\mathbf{v}\,d\gamma_F\\ &= \frac{-1}{We}\int_{\Gamma_F(t)} \underline{\nabla} id_{\Gamma_F} : \underline{\nabla}\mathbf{v}\,d\gamma_F\\ &\quad + \frac{1}{We}\int_{cl(t)} (\boldsymbol{\nu}_{cl}\cdot\underline{\nabla} id_{\Gamma_F})\cdot\mathbf{v}d\zeta\\ &= \frac{-1}{We}\int_{\Gamma_F(t)} \underline{\nabla} id_{\Gamma_F} : \underline{\nabla}\mathbf{v}\,d\gamma_F\\ &\quad + \frac{1}{We}\int_{cl(t)} \boldsymbol{\nu}_{cl}\cdot\mathbf{v}d\zeta,\end{aligned}$$

since $\boldsymbol{\nu}_{cl}\cdot\underline{\nabla} id_{\Gamma_F} = \boldsymbol{\nu}_{cl}$. Here, the identity mapping $id_{\Gamma_F} : \mathbb{R}^d \mapsto \mathbb{R}^d$ is the restriction onto $\Gamma_F(t)$, $\boldsymbol{\nu}_{cl}$ is the outward unit normal vector at the moving contact line $cl(t)$ with respect to the free surface $\Gamma_F(t)$. Now, we decompose the test function in the contact line integral as

$$\mathbf{v} = (\mathbf{v}\cdot\boldsymbol{\nu}_S)\boldsymbol{\nu}_S + \sum_{i=1}^{2}(\mathbf{v}\cdot\boldsymbol{\tau}_{i,S})\boldsymbol{\tau}_{i,S}$$

and use the fact that $\mathbf{v}\cdot\boldsymbol{\nu}_S = 0$ on Γ_S to get

$$\begin{aligned}\int_{cl(t)} \boldsymbol{\nu}_{cl}\cdot\mathbf{v}d\zeta &= \int_{cl(t)} (\boldsymbol{\nu}_{cl}\cdot\boldsymbol{\tau}_{i,S})(\mathbf{v}\cdot\boldsymbol{\tau}_{i,S})d\zeta\\ &= \int_{cl(t)} \cos(\theta)\ \mathbf{v}\cdot\boldsymbol{\tau}_{i,S}d\zeta, \qquad (5)\end{aligned}$$

since $\boldsymbol{\nu}_{cl}\cdot\boldsymbol{\tau}_{i,S} = \cos(\theta)$. Thus, the external force term $f(\mathcal{K},\mathbf{v})$ in the weak form (4) becomes

$$\begin{aligned}f(\mathcal{K},\mathbf{v}) &= \frac{1}{Fr}\int_{\Omega(t)} \mathbf{e}\cdot\mathbf{v}\,dx\\ &\quad - \frac{1}{We}\int_{\Gamma_F(t)} \underline{\nabla} id_{\Gamma_F} : \underline{\nabla}\mathbf{v}\,d\gamma_F\\ &\quad + \frac{1}{We}\int_{cl(t)} \cos(\theta)\ \mathbf{v}\cdot\boldsymbol{\tau}_{i,S}d\zeta,\end{aligned}$$

which contains the contact angle θ. Another advantage of using this technique is that only first order derivatives (tangential gradient) are needed to approximate the curvature. Further, this approximation can be done with the standard finite element basis functions.

3 Numerical scheme

A finite element scheme with Arbitrary Lagrangian Eulerian (ALE) approach is used to solve the considered test examples. We refer to [6] for more details of the numerical scheme. Here, we briefly describe the main ingredients of our numerical scheme.

3.1 Discretisation

First, we reformulate the weak form in an axisymmetric weak form and reduce one space dimension. Then, after rewriting the weak form in the ALE framework, we triangulate the meridian domain of the axisymmetric droplet $\Omega(t)$ with a boundary resolved triangular mesh. We take the "inf-sup" stable second order finite element pair $P_2^{\text{bubble}}/P_1^{\text{disc}}$ for the velocity and pressure, where the velocity space is enriched with a cubic bubble function [2]. For the time discretisation we use the second order, strongly A-stable fractional-step-ϑ scheme. Then, the convection term is linearised by an iteration of fixed point type. Since it is difficult to maintain the hierarchy of mesh levels for moving grids, especially when remeshing is needed, we prefer to take a direct solver for solving the linear system of equations.

3.2 Tracking the free surface

After calculating the velocity and pressure at each time step, we advect the (free surface and interface) boundary points with the fluid velocity in a Lagrangian manner. Then, the inner points are displaced with the elastic solid technique according to the displacement of the boundary points.

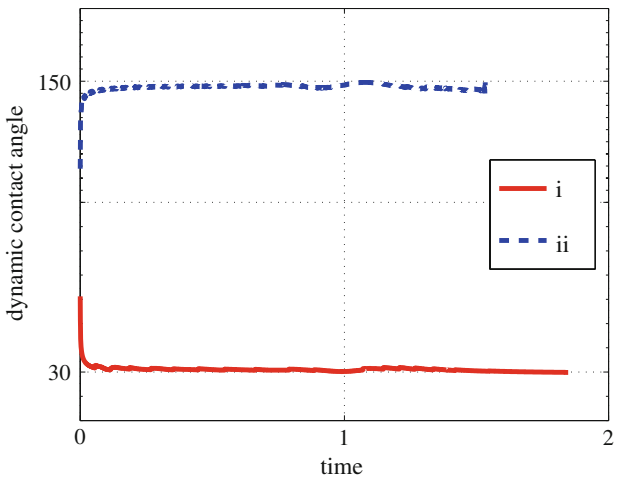

Fig. 2 Dynamic contact angle of an axisymmetric spreading droplet with $Re = 100$ and $We = 1.4$. (i) $\theta_e = 30°$, (ii) $\theta_e = 150°$

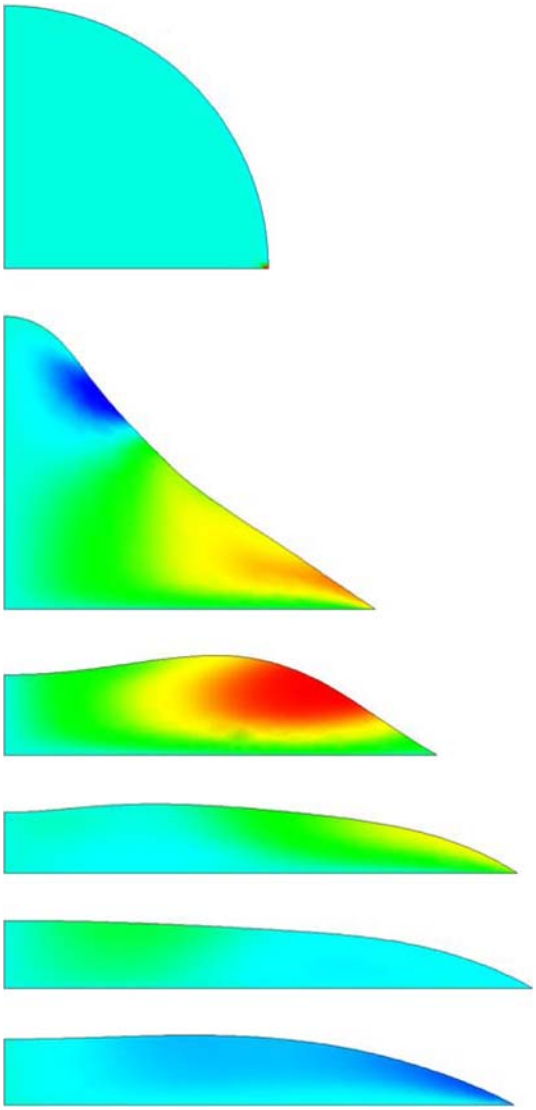

Fig. 3 A sequence of images at different instances of an axisymmetric spreading droplet with $\theta_e = 30°$, timings from image 1 are $t = 0,\ 0.5,\ 1.0,\ 1.5,\ 2.0,\ 2.5$. *Colours* represent the magnitude of the velocity in radial direction, min $= -0.4$ (*blue*) max $= 0.9$ (*red*)

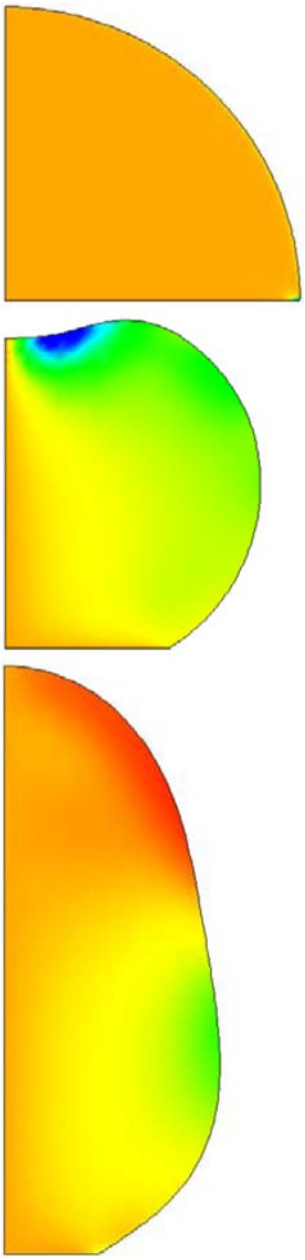

Fig. 4 A sequence of images at different instances of an axisymmetric spreading droplet with $\theta_e = 150°$, timings from image 1 are $t = 0,\ 0.5,\ 1.0$. *Colours* represent the magnitude of the velocity in radial direction, min $= -1.4$ (*blue*) max $= 0.5$ (*red*)

4 Numerical results

To investigate the implementation of the contact angle in the proposed numerical scheme we made an array of computations for spreading and oscillating pendant liquid droplets. Computations are made until a prescribed time or until the droplet attaining the equilibrium position. For the validation of the numerical scheme we refer to [6]. In the following examples, the computations have been started at time $t = 0$ with a mesh with $h_{\min} = 0.001032$ and $h_{\max} = 0.1278$ corresponding to 10, 670 and 5, 034 degrees of freedom for velocity and pressure, respectively. If remeshing is needed, an automatic mesh generator implemented in our code generates a new mesh in such a way that the area of each cell is less or equal to 0.005. These quantities slightly vary over time, due to the moving mesh and the remeshing. The time step has been set to 0.0001. One or two fixed-point iterations in each sub-step of the fractional-step-ϑ scheme have been sufficient to reduce the residual under the threshold of 10^{-8}. We found that the additional time needed for calculating the new mesh positions by the elastic mesh update, the mesh velocity, generating the mass and stiffness matrices, and the right hand

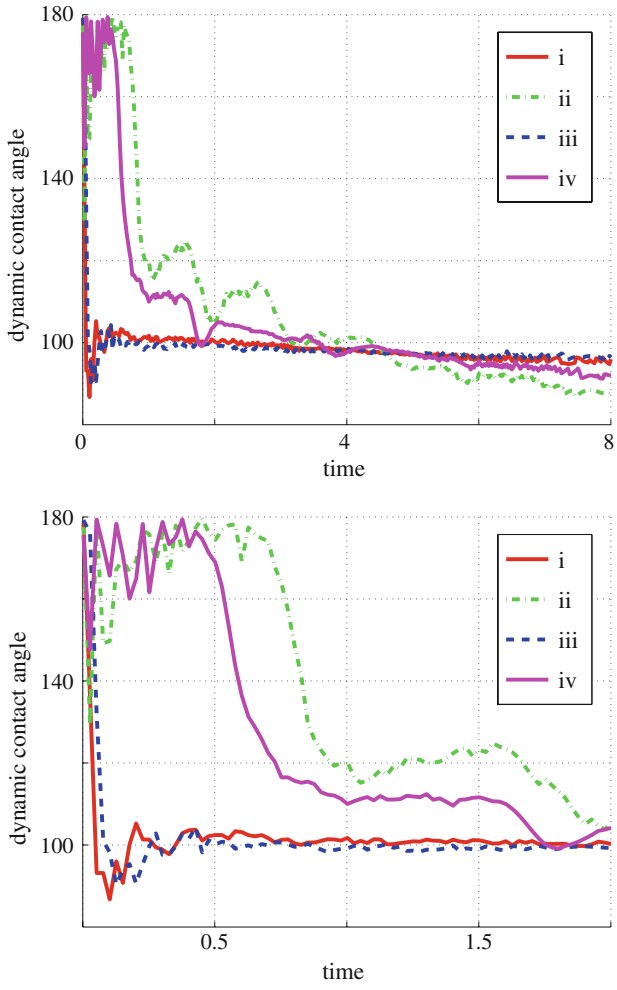

Fig. 5 Dynamic contact angle of an axisymmetric water droplet impinging on a wax surface with $\theta_e = 100°$, $Re = 4204$, $We = 90$ and $Fr = 93$. (*i*) $1/\beta_\epsilon = 1$, (*ii*) $1/\beta_\epsilon = 10$, (*iii*) $1/\beta_\epsilon = 1/r$ and (*iv*) $1/\beta_\epsilon = 10/r$

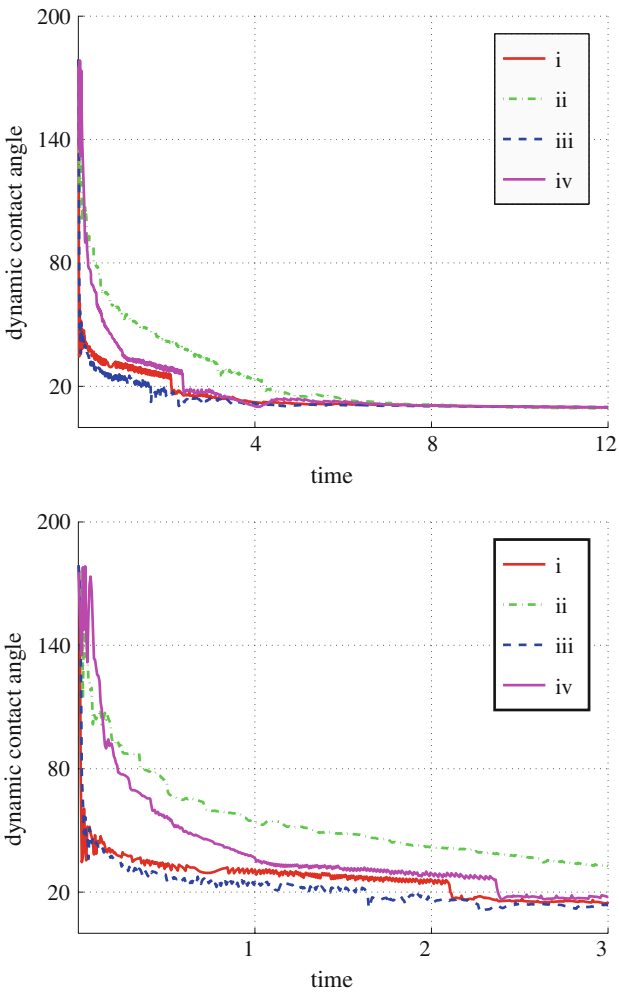

Fig. 6 Dynamic contact angle of an axisymmetric water droplet impinging on a smooth glass with $\theta_e = 10°$, $Re = 4204$, $We = 90$ and $Fr = 93$. (*i*) $1/\beta_\epsilon = 1$, (*ii*) $1/\beta_\epsilon = 10$, (*iii*) $1/\beta_\epsilon = 1/r$ and (*iv*) $1/\beta_\epsilon = 10/r$

side, compared to a simple flow calculation on a fixed grid, is only a small fraction, i.e., the time for solving the fixed point iteration dominates the overall procedure.

4.1 Spreading droplet

We consider a water droplet of radius $r_0 = 100$ µm in zero gravity space which resides on a horizontal solid surface with a contact angle $\theta = 90°$. That is, at time $t = 0$ the domain of the droplet is the semi-sphere of radius $r_0 = 100$ µm. For water, the following values are used: surface tension $\sigma = 0.073$ N/m, density $\rho = 1,000\,\mathrm{kg/m^3}$, the dynamic viscosity $\mu = 10^{-3}$ N s/m^2. The used characteristic values are $L = r_0$ and $U = 1$ m/s which result in the dimensionless numbers $Re = 100$ and $We = 1.4$. In these computations we use $1/\beta_\epsilon = 1$ and assume that the droplet is in rest at $t = 0$.

For the droplet with the data above, we changed the equilibrium contact angles to $\theta_e = 30°$ and $\theta_e = 150°$, respectively. Since the free surface of the droplet before changing the equilibrium contact angle has been in the equilibrium position and there are no other external forces (initial velocity is zero and gravitational force is neglected), the only imbalances in forces at time $t = 0$ is at the contact line because of $\theta(t = 0) \neq \theta_e$. Thus, if the contact angle is incorporated in the numerical scheme accurately then the droplet should starts to spread or recoil according to the equilibrium contact angle. As we expected, in the first case the droplet starts to spread ($\theta(t = 0) > \theta_e$) and in the second case the droplet starts to recoil ($\theta(t = 0) < \theta_e$). The measured dynamic contact angle from the geometry of the moving mesh is presented in Fig. 2 for both cases. Figures 3 and 4 show sequences of frames corresponding to different instance of the first and second cases, respectively. The colours in these

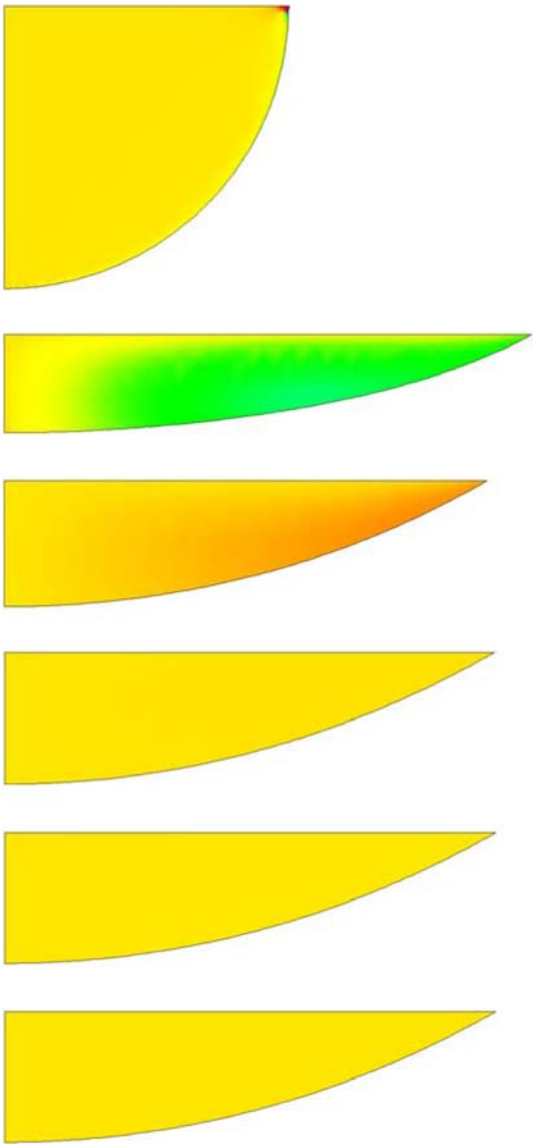

Fig. 7 A sequence of images at different instances of an axisymmetric pendant droplet with $\theta_e = 30°$, timings from image 1 are $t = 0,\ 1.0,\ 2.0,\ 3,\ 4,\ 5$. *Colours* represent the magnitude of the velocity in radial direction, min $= -1.2$ (*blue*) max $= 0.3$ (*red*)

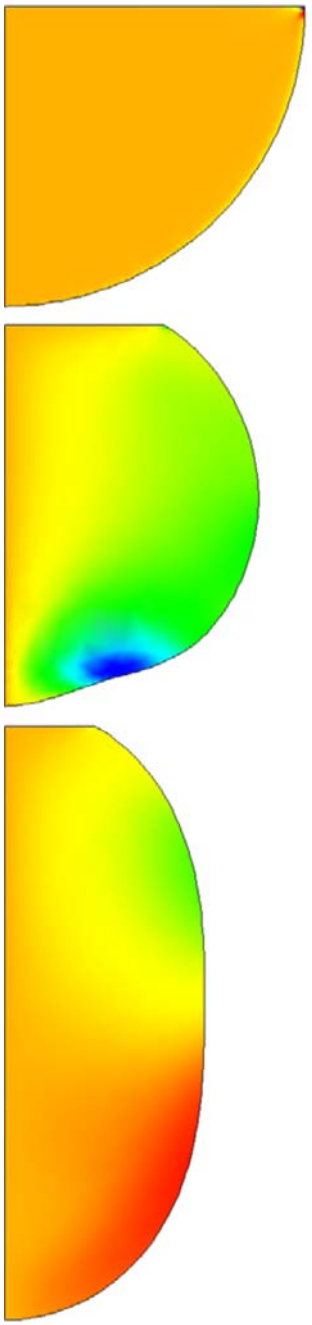

Fig. 8 A sequence of images at different instances of an axisymmetric pendant droplet with $\theta_e = 150°$, timings from image 1 are $t = 0,\ 0.5,\ 1.0$. *Colours* represent the magnitude of the velocity in radial direction, min $= -1.6$ (*blue*) max $= 0.3$ (*red*)

images represent the magnitude of the velocity in the radial direction. The computed results of both cases show that the numerical scheme incorporates the given contact angle accurately.

4.2 Effects of the slip coefficient on the dynamic contact angle

Since the exact value of the slip coefficient is unknown, a few computations are made to study the effects of the slip coefficient on the dynamic contact angle. In this example, we consider a spherical water droplet of radius $r_0 = 1.35$ mm impinging perpendicularly on a wax surface with the impact velocity $\mathbf{u}(0) = 1.56$ m/s. Further, the used equilibrium contact angle is $\theta_e = 100°$. The dimensionless numbers with $L = 2r_0$ and $U = 1.56$ m/s are $Re = 4204$, $We = 90$ and $Fr = 93$. We compute this example with the following four different values of the slip coefficient: (i) $1/\beta_\epsilon = 1$, (ii) $1/\beta_\epsilon = 10$, (iii) $1/\beta_\epsilon = 1/r$ and (iv) $1/\beta_\epsilon = 10/r$. The dynamic contact angle obtained in this array of computations

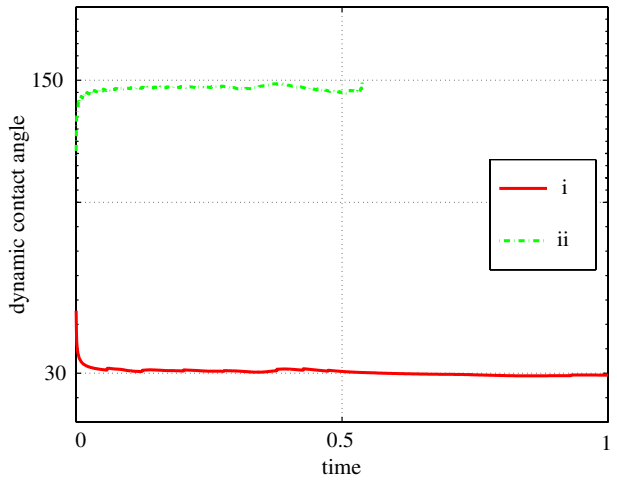

Fig. 9 Dynamic contact angle of an axisymmetric pendant droplet with $Re = 100$, $We = 1.4$ and $Fr = 1020$. (*i*) $\theta_e = 30°$, (*ii*) $\theta_e = 150°$

is shown in Fig. 5. Next, for the same droplet configurations but with a different equilibrium contact angle $\theta_e = 10°$, we perform another array of computations to study the effects of the slip coefficient on the dynamic contact angle on a hydrophilic surface. The different dynamic contact angles obtained in these computations are presented in Fig. 6.

These results clearly show the influence of the slip coefficient on the contact angle on both the hydrophobic and hydrophilic surfaces. However, in comparison with the hydrophilic surface, the influence is less for a hydrophobic surface (note the different scaling in Figs. 5, 6).

4.3 Pendant droplet

Further, to show the robustness of the numerical scheme we compute the oscillating pendant liquid droplet including gravitational effects. Here, we consider a water droplet of radius $r_0 = 50$ µm hanging on a horizontal surface as the initial configuration.

At time $t = 0$, the droplet is assumed to be of semi-spherical shape, i.e., $\theta(t = 0) = 90°$ and in rest. The computational domain is the meridian domain of the semi-spherical droplet. We use the slip coefficient $1/\beta_\epsilon = 1$, characteristic length $L = 2r_0$ and characteristic velocity $U = 1$ m/s. These values result in $Re = 100$, $We = 1.4$ and $Fr = 1020$. As in the spreading droplet case we make two different computations with $\theta_e = 30°$ and $\theta_e = 150°$. Sequences of images obtained in the pendant droplet computations at different instance for the two cases, $\theta_e = 30°$ and $\theta_e = 150°$, are shown in Figs. 7 and 8, respectively. The colours in these images indicate the magnitude of the velocity in radial direction. Figure 9 shows the obtained dynamic contact angle of the pendant droplet in both cases. These results once again show that the contact angle is accurately incorporated in the numerical scheme.

5 Concluding remarks

A new finite element scheme, which allows to compute the dynamic contact angle for a given equilibrium contact angle in moving contact line problems is presented. The capability to capture the dynamics of the contact angle and the robustness of the numerical scheme are shown through the examples of spreading and pendant liquid droplets. Further, we have observed the dependency of the dynamic contact angle on the slip coefficient.

References

1. Bänsch, E.: Numerical methods for the instationary Navier–Stokes equations with a free capillary surface. Habilitationsschrift, Albert-Ludwigs Universität (2001)
2. Crouzeix, M., Raviart, P.A.: Conforming and nonconforming finite element methods for solving the stationary Stokes equations I. R.A.I.R.O. Anal. Numér. **7**, 33–76 (1973)
3. Dziuk, G.: An algorithm for evolutionary surfaces. Numer. Math. **58**, 603–611 (1991)
4. Eggers, J., Stone, H.A.: Characteristic lengths at moving contact lines for a perfectly wetting fluid: the influence of speed on the dynamic contact angle. J. Fluid Mech. **505**, 309–321 (2004)
5. Fukai, J., Shiiba, Y., Yamamoto, T., Miyatake, O., Poulikakos, D., Megaridis, C.M., Zhao, Z.: Wetting effects on the spreading of a liquid droplet colliding with a flat surface: experiment and modeling. Phys. Fluids **7**(2), 236–247 (1995)
6. Ganesan, S.: Finite element methods on moving meshes for free surface and interface flows. Ph.D. Thesis, Otto-von-Guericke-Universität, Fakultät für Mathematik, Magdeburg (2006)
7. Lauga, E., Brenner, P., Stone, H.A.: Microfluidics: the no-slip boundary condition. In: Foss, J., Tropea, C., Yarin, A. (eds.) Handbook of Experimental Fluid Dynamics. Springer, New York (2007)
8. Matthies, G.: Finite element methods for free boundary value problems with capillary surfaces. Ph.D. Thesis, Otto-von-Guericke-Universität, Fakultät für Mathematik, Magdeburg (2002)
9. Renardy, M., Renardy, Y., Li, J.: Numerical simulation of moving contact line problems using a volume-of-fluid method. J. Comput. Phys. **171**, 243–263 (2001)
10. Ruschak, K.: A method for incorporating free boundaries with surface tension in finite element fluid-flow simulators. Int. J. Numer. Meth. Eng. **15**, 639–648 (1980)
11. Spelt, P.D.M.: A level-set approach for simulations of flows with multiple moving contact lines with hysteresis. J. Comput. Phys. **207**, 389–404 (2005)
12. Šikalo, Š., Wilhelm, H.D., Roisman, I.V., Jakirlić, S., Tropea, C.: Dynamic contact angle of spreading droplets: experiments and simulations. Phys. Fluids **17**(062103), 1–13 (2005)